Cell Reports

Article

Identification and Characterization of a Transcribed Distal Enhancer Involved in Cardiac *Kcnh2* Regulation

Graphical Abstract

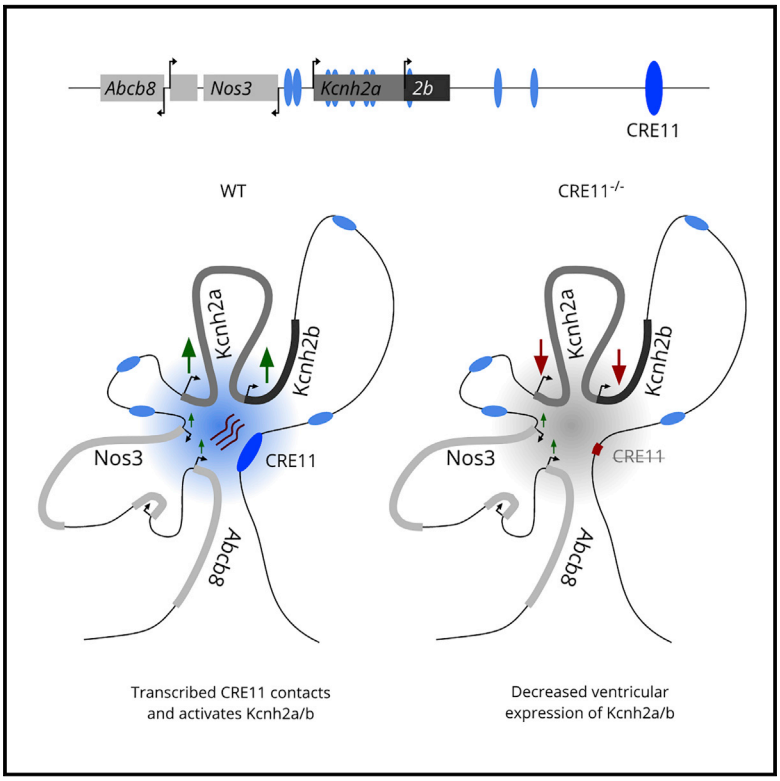

Authors

Malou van den Boogaard, Jan Hendrik van Weerd, Amira C. Bawazeer, ..., Phil Barnett, Jeroen Bakkers, Vincent M. Christoffels

Correspondence

v.m.christoffels@amsterdamumc.nl

In Brief

KCNH2 encodes a potassium channel critical for cardiac repolarization. Van den Boogaard et al. identified a transcribed cardiac-specific enhancer physically contacting *Kcnh2.* Genomic deletion by CRISPR/Cas9 caused a modest decrease in ventricular *Kcnh2a* and *Kcnh2b* expression, demonstrating the complexity of the regulatory landscape regulating *Kcnh2* expression.

Highlights

- Multiple active regulatory elements are identified within the *Kcnh2* locus
- A transcribed enhancer physically contacts two *Kcnh2* promoters specifically in the heart
- Knockdown of the RNA transcript from this element leads to decreased *Kcnh2b* expression
- Genomic deletion in mice causes a modest decrease in ventricular *Kcnh2* expression

van den Boogaard et al., 2019, Cell Reports *28*, 2704–2714
September 3, 2019
https://doi.org/10.1016/j.celrep.2019.08.007

CellPress

OPEN ACCESS
CellPress

Cell Reports
Article

Identification and Characterization of a Transcribed Distal Enhancer Involved in Cardiac *Kcnh2* Regulation

Malou van den Boogaard,[1,5] Jan Hendrik van Weerd,[1,5] Amira C. Bawazeer,[1] Ingeborg B. Hooijkaas,[1] Harmen J.G. van de Werken,[2,3,4] Federico Tessadori,[4] Wouter de Laat,[4] Phil Barnett,[1] Jeroen Bakkers,[4] and Vincent M. Christoffels[1,6,*]

[1]Amsterdam UMC, University of Amsterdam, Department of Medical Biology, Amsterdam Cardiovascular Sciences, 1105AZ Amsterdam, the Netherlands
[2]Cancer Computational Biology Center, Erasmus MC Cancer Institute, Erasmus University Medical Center, 3015 GD, Rotterdam, the Netherlands
[3]Department of Urology, Erasmus MC Cancer Institute, Erasmus University Medical Center, 3015 GD, Rotterdam, the Netherlands
[4]Hubrecht Institute-KNAW and University Medical Center Utrecht, Utrecht, the Netherlands
[5]These authors contributed equally
[6]Lead Contact
*Correspondence: v.m.christoffels@amsterdamumc.nl
https://doi.org/10.1016/j.celrep.2019.08.007

SUMMARY

The human ether-a-go-go-related gene *KCNH2* encodes the voltage-gated potassium channel underlying I_{Kr}, a current critical for the repolarization phase of the cardiac action potential. Mutations in *KCNH2* that cause a reduction of the repolarizing current can result in cardiac arrhythmias associated with long-QT syndrome. Here, we investigate the regulation of *KCNH2* and identify multiple active enhancers. A transcribed enhancer ~85 kbp downstream of *Kcnh2* physically contacts the promoters of two *Kcnh2* isoforms in a cardiac-specific manner *in vivo*. Knockdown of its ncRNA transcript results in reduced expression of *Kcnh2b* and two neighboring mRNAs, *Nos3* and *Abcb8, in vitro.* Genomic deletion of the enhancer, including the ncRNA transcription start site, from the mouse genome causes a modest downregulation of both *Kcnh2a* and *Kcnh2b* in the ventricles. These findings establish that the regulation of *Kcnh2a* and *Kcnh2b* is governed by a complex regulatory landscape that involves multiple partially redundantly acting enhancers.

INTRODUCTION

The human ether-a-go-go-related gene (*hERG* or *KCNH2*) encodes the voltage-gated potassium channel that underlies the rapidly activating delayed rectifier current I_{Kr} (Sanguinetti et al., 1995; Trudeau et al., 1995). I_{Kr} is a major contributor to the repolarization phase of the action potential in human cardiomyocytes (Sanguinetti and Jurkiewicz, 1990). Misregulation of this current results in slowing of ventricular repolarization and QT prolongation. When these events occur because of mutations in *KCNH2*, the condition is diagnosed as long-QT syndrome type 2 (LQTS type 2 or LQT2), a life-threatening heritable arrhythmia that often leads to polymorphic ventricular tachycardia and, ultimately, sudden cardiac death (SCD) in young patients (Sanguinetti, 2010). Despite the characterization of *KCNH2* and several other genes as molecular substrate for LQTS, there is a high degree of unexplained phenotypic variability in the disease, even between family members carrying the same mutation (Giudicessi and Ackerman, 2013).

Genome-wide association studies revealed common variants in non-coding genomic regions close to *KCNH2* to be associated with QT interval duration (Arking et al., 2014; Méndez-Giráldez et al., 2017; Newton-Cheh et al., 2009; Pfeufer et al., 2009), indicating that small perturbations affecting the tight control of *KCNH2* levels can have significant implications for cardiac function. In the human genome, five different *KCNH2* transcripts have been reported to be transcribed from the *KCNH2* locus, which vary considerably in distribution and expression level (Guasti et al., 2008; Huffaker et al., 2009; Kupershmidt et al., 1998; Lees-Miller et al., 1997; London et al., 1997; Trudeau et al., 1995). At least three of these isoforms—*KCNH2A*, *KCNH2B*, and *KCNH2uso*—play a functional role in the human heart. *KCNH2A* and *KCNH2B* are highly conserved among species. Both transcripts represent different *KCNH2* isoforms that together can form variable heteromeric hERG channels (Larsen et al., 2008; Sale et al., 2008). Tissue-specific RNA expression in mice revealed that *Kcnh2a* is abundantly expressed in murine heart, brain, lung, and testis, whereas *Kcnh2b* expression is more cardiac specific (Lees-Miller et al., 1997; London et al., 1997). Selective knockdown of *Kcnh2b* eliminates I_{Kr} from adult ventricular cardiomyocytes and elicits episodes of sinus bradycardia (Lees-Miller et al., 2003). *KCNH2uso* does not form functional hERG channels and is not conserved among species (Gong et al., 2014).

The high degree of phenotypical heterogeneity in LQTS patients might be rooted in the complex interplay between multiple direct and indirect factors involved in the differential

transcriptional regulation of the separate isoforms that form the heteromeric hERG channels. Regulation of gene expression is mediated by *cis*-regulatory elements (CREs), which physically contact gene promoters through DNA looping and act together to stimulate or repress mRNA transcription by influencing promoter activity (Andrey and Mundlos, 2017; de Laat and Duboule, 2013). As such, they play an important role in the spatiotemporal regulation of gene expression. Additionally, there is increasing evidence that non-coding RNAs (ncRNAs) arise from genomic locations where CREs are found (e.g., intragenic regions, UTRs, enhancers) (De Santa et al., 2010; Kim et al., 2010; Mercer et al., 2009). Depending on their specific subtypes, ncRNAs have been demonstrated to be involved in, among others, gene regulation, DNA replication, mRNA translation and stability, alternative splicing, and protein trafficking (Archer et al., 2015; Boon et al., 2016; Hofmann and Boon, 2014; Kopp and Mendell, 2018; Rothschild and Basu, 2017). Thus, aberrant expression of ncRNAs can have functional consequences for specific disease states, which makes ncRNAs interesting targets for novel therapies.

The potential differential regulation of *KCNH2A* and *KCNH2B* could have important implications for future therapeutic strategies. Therefore, we aimed to investigate the regulatory landscape near *Kcnh2*. We identified and characterized several candidate CREs and provide evidence that a subset of these elements is in close physical proximity to the *Kcnh2* promoters specifically in the heart and has regulatory potential both *in vitro* and *in vivo*. We show that a ncRNA transcribed from one of these CREs is involved in the cardiac expression of *Kcnh2b* and two neighboring mRNAs, *Nos3* and *Abcb8*, in cultured HL-1 cells. CRISPR/Cas9-mediated deletion of this genomic region from the mouse genome decreased the ventricular expression of both *Kcnh2a* and *Kcnh2b in vivo.* We present a map of the regulatory landscape surrounding *Kcnh2* and provide evidence that a downstream regulatory sequence, expressing a ncRNA, is involved in the regulation of expression of the two *Kcnh2* isoforms.

RESULTS

Identification of Regulatory Elements in the *Kcnh2* Locus

The *KCNH2* locus harbors multiple common variants associated with LQTS (Arking et al., 2014). We analyzed publicly available Hi-C data on lymphoblastoid cells (Rao et al., 2014) and found that the majority of these variants is located in non-coding regions within a topologically associating domain (TAD) delineated by binding sites for CTCF, a factor involved in the structural organization of the genome (Ghirlando and Felsenfeld, 2016; Holwerda and de Laat, 2013) (Figure S1). Variants in non-coding DNA are likely to affect CREs (Maurano et al., 2012). We used the enhancer prediction tool EMERGE (van Duijvenboden et al., 2015), integrating publicly available chromatin immunoprecipitation sequencing (ChIP-seq) datasets of cardiac transcription factors and of proteins associated with active regulatory sequences and active transcription, to identify CRE candidates in both the human and mouse locus. On the basis of this prediction, we selected 11 conserved putative cardiac CREs located within the *Kcnh2* locus, the boundaries of which we demarcated by the location of CTCF binding sites and by the borders of the TAD (Figures 1A and 1B). To assess their regulatory potential, we tested the murine candidate CREs by luciferase reporter assays after transfection in three different cell lines: HepG2, a hepatocellular carcinoma derived cell line; HEK293T, a human embryonic kidney cell line; and HL-1, a mouse atrial cardiomyocyte-like cell line. CRE3, CRE9, and CRE11 showed strong activity in all three cell types, whereas CRE1, CRE4, and CRE6-CRE10 drove reporter activity in HL-1 cells, albeit to a lesser extent (Figure 1C). We did not observe a correlation between activity in HL-1 cells and EMERGE signal strength predicting cardiac CREs (e.g., compare CRE6 activity and signal). CREs, as identified by EMERGE (epigenetic data), represent regulatory elements with different functions, only a subset of which have the property to enhance expression in transfection assays. These results indicate that multiple CRE candidates close to *Kcnh2* hold regulatory potential in different cell lines.

To test the regulatory potential of these regions *in vivo*, all 11 candidates were tested in zebrafish using the ZED vector system, which allows simultaneous screening of transgenesis and RE-driven activity using two fluorescent markers (Bessa et al., 2009). CRE7, CRE9, and CRE11, active *in vitro*, showed regulatory activity in the zebrafish heart, whereas CRE3 did not display any cardiac regulatory activity *in vivo* (Figure 1D). CRE5 and CRE8 repressed cardiac reporter activity. We measured the regulatory potential of the conserved human homologs of active regions CRE1, CRE3, CRE7, CRE9, and CRE11 in HEK293T and HL-1 cells. Except for CRE9, all tested human CREs drove luciferase activity in both cell lines, indicating conserved regulatory activity of these regions (Figure 1E). Of all tested CRE candidates, CRE11 was shown to hold the strongest regulatory potential *in vitro* (both human and murine homologs) and *in vivo* in zebrafish, and as such was identified as a promising candidate to regulate *Kcnh2* expression. Analysis of available ChIP-seq datasets revealed that CRE11 is bound by multiple transcription factors important for cardiac development, including the T-box transcription factor Tbx20 (Figure S2A) (Boogerd et al., 2018), which was shown to control the expression of *Kcnh2* in human cardiomyocytes (Caballero et al., 2017). Furthermore, it is marked by H3K4me3, a histone modification mark predominantly associated with active transcription (Heintzman et al., 2007; Lauberth et al., 2013; Yue et al., 2014). Increased H3K4me3 on non-coding DNA has been associated with increased levels of transcription of both the RE and nearby protein-coding genes (Barski et al., 2007; Clouaire et al., 2012; Pekowska et al., 2011).

Cardiac-Enriched Contact Frequency between CRE11 and the Promoters of *Kcnh2* and *Nos3*

Transcriptional regulation of target genes by CREs requires their physical proximity (de Laat and Duboule, 2013). To investigate the physical proximity between the *Kcnh2* gene promoters and putative CREs in the region, we deployed high-resolution chromosome conformation capture sequencing (4C-seq) (van de Werken et al., 2012). We used murine hepatic tissue as a control in addition to cardiac tissue to find specific cardiac interactions. The viewpoints (bait) were set on the *Kcnh2* promoter isoform A

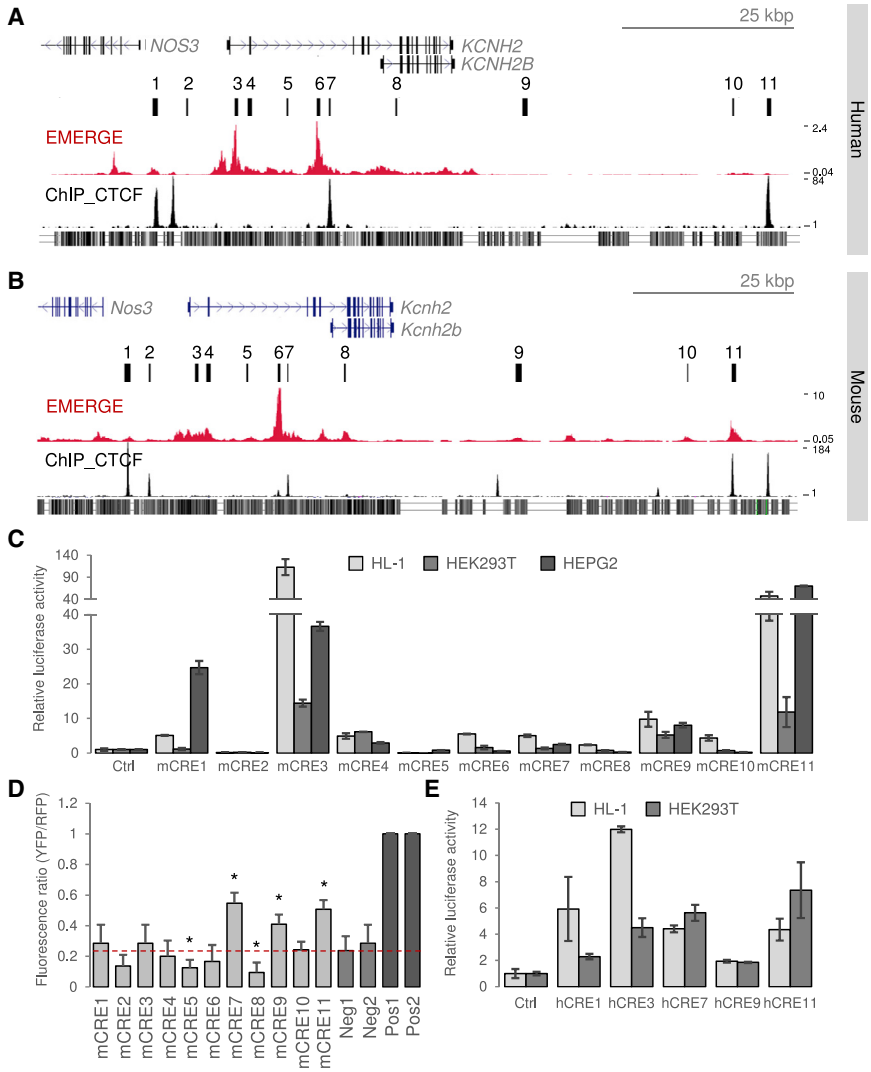

Figure 1. Identification and Functional Characterization of Regulatory Elements in the *KCNH2* Locus

(A) UCSC Genome Browser view of the human *KCNH2* locus. The EMERGE track depicts predicted cardiac enhancers on the basis of integrated cardiac-specific datasets. Numbers 1–11 indicate putative *cis*-regulatory elements (CREs) within CTCF sites chosen for further testing.

(B) UCSC Genome Browser view of the murine *KCNH2* locus with EMERGE-predicted CREs. GERP depicts conservation between species.

(C) Regulatory activity of putative murine REs in HL-1, HEK293T, and HepG2 cells. Luciferase values of CRE candidates are normalized to the activity of the empty pGL2-SV40 vector (Ctrl). *$p < 0.05$.

(D) Ratio of GFP expression (enhancer activity) over RFP expression (genomic integration of the construct) in hearts of zebrafish for each putative CRE. CRE7, CRE9, and CRE11 activate cardiac GFP expression, whereas CRE5 and CRE8 seem to repress basal activity of the ZED vector. Neg1 (reference) and Neg2 represent the empty ZED vector and a validated neuronal regulator element *Cadps*, respectively. Pos1 and Pos2 represent validated cardiac regulatory elements for *Scn5a* and *cTnT*. *$p < 0.05$.

(E) Regulatory of human orthologs of *in vivo* active CREs in HL-1 and HEK293T cells. Luciferase values of CRE candidates are normalized to the activity of the empty pGL2-SV40 vector (Ctrl). Error bars represent SD. See also Figures S1 and S2A.

(*Kcnh2a*) and the most promising candidate, CRE11. We observed a similar interaction profile from both viewpoints and clear interactions between the viewpoints in both heart and liver samples (Figure 2; Figure S2C). *Kcnh2* is expressed only at low levels in developing liver (de Castro et al., 2006) and is not expressed in adult liver (London et al., 1997).

The similar contact profiles and the fixed spatial proximity of CRE11 with *Kcnh2* in both heart and liver tissue therefore suggests that CRE11 is not recruited to the promoter upon initiation of transcription but rather that the *Kcnh2* regulatory domain is organized in a pre-established, permissive organization, independent of tissue type (de Laat and Duboule, 2013). Nevertheless, quantitative analysis of the interactions revealed an increased interaction frequency between CRE11 and *Kcnh2a* in cardiac tissue compared with liver (Figures 2B and 2C). Closer inspection of this contact region shows that it is broad (±10 kbp) and extends from CRE11 toward CRE10. Other interactions with the *Kcnh2a* viewpoint included the region around CRE9, with a similar distribution of interactions in heart and liver samples, and with the region containing CRE5–8, although this region is too close to the viewpoint to extract any tissue-specific interactions (Figures 2A and 2C). From the CRE11 viewpoint we found that the region of CRE6 to CRE8, which contains the alternative promoter for *Kcnh2* isoform B (*Kcnh2b*), is more frequently contacted in cardiac tissue. The contact profile from the CRE11 viewpoint furthermore suggests that there are multiple sites of interaction upstream of the *Kcnh2a* transcription start site, including particularly strong and cardiac-enriched interactions with the *Kcnh2a* and *Nos3* promoter. Other interactions were found near *Atg9b*, *Abcb8*, *Cdk5*, and *Agap3* upstream of the viewpoint and near *Nupl2* downstream of the viewpoint (Figure 2; Figure S3). These data indicate that the TAD containing *Kcnh2* and *CRE11* is approximately 0.3 Mbp in size and includes 11 genes, among which are several genes that are functionally active in the adult heart, including *Kcnh2*, *Nos3*, *Abcb8*, and *Asic3* (Cheng et al., 2014; Ichikawa et al., 2012; Scherrer-Crosbie et al., 2001). Furthermore, these findings suggest that CRE11, located ~85 kbp downstream of the transcription start site of *Kcnh2*, is an active CRE and in close spatial proximity to the promoters of both *Kcnh2* isoforms and of *Nos3*.

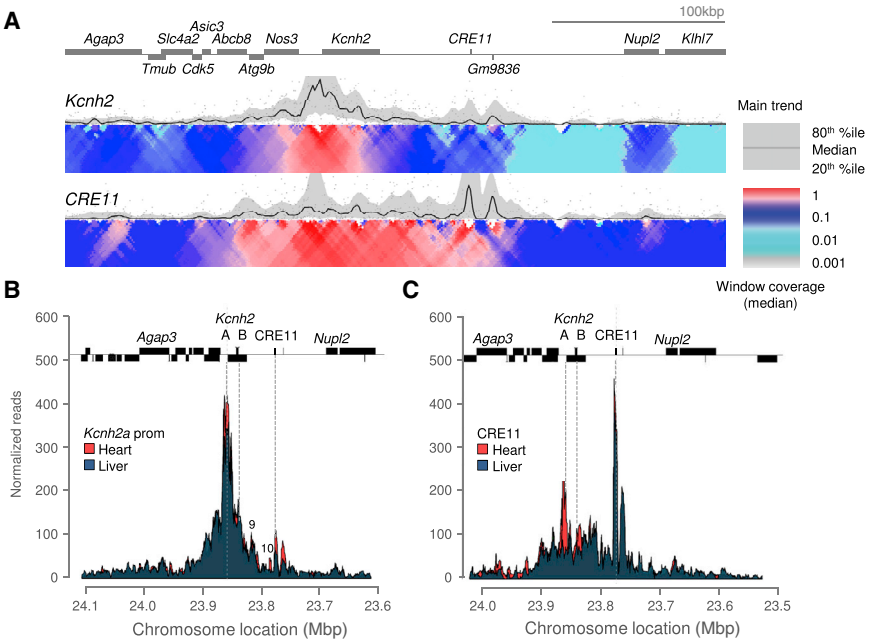

Figure 2. Overview of the Genomic Architecture of the *Kcnh2* Contact Profiles

(A) Normalized contact intensities (gray dots) and their running median trends (black line) are depicted for the viewpoint in *Kcnh2* and CRE11. Medians are computed for 4 kbp windows, and the gray band displays the 20th–80th percentiles for these windows. Below the profile, statistical enrichment across differently scaled window sizes (from 2 kbp [top row] to 50 kbp [bottom row]) is depicted of the observed number of sequenced ligation products over the expected total coverage of captured products, with the latter being estimated on the basis of a probabilistic background model. Local changes in color codes indicate regions statistically enriched for captured sequences, which correspond to the promoter-enhancer contacts described. The gray 80th percentile band and color codes in the CRE11 viewpoint tract show contacts with the *Kcnh2* promoters and many other regions in the TAD. From the promoter region of *Kcnh2a*, the most prominent interaction is seen with the location of CRE11.

(B and C) Overlap of heart (red) and liver (blue) contact profiles for the *Kcnh2a* promoter (B) and CRE11 (C) viewpoints reveal contact frequencies between these two regions are enriched in heart tissue (gray dashed lines).

See also Figure S2C.

A Bidirectionally Transcribed ncRNA Overlapping CRE11 Is Abundantly Expressed in Several Tissues in Mouse

Active CREs are frequently accompanied by transcriptional activity at their location, often in a bidirectional manner (Arner et al., 2015; Kim et al., 2010). Most of these transcripts are dynamic and unstable (Andersson et al., 2014), but a small subset of CREs produce stable long ncRNAs that may play roles in the regulation of gene expression (Kim et al., 2010; Larsen et al., 2008; Li et al., 2013). This prompted us to investigate whether such transcripts are present at the location of CRE11. As *Kcnh2* is expressed in a variety of tissues, including the intestine (Farrelly et al., 2003), brain (Huffaker et al., 2009), and kidney (Carrisoza et al., 2010), we measured expression levels in multiple adult mouse tissues for *Kcnh2* isoforms and *CRE11* transcript. In concordance with previous studies, we observed that *Kcnh2* (combined product of isoform A and B) expression is highest in brain, specifically cerebellum, and heart (Figure 3A) (London et al., 1997). For both separate isoforms, expression was higher in atria compared with ventricles (Marionneau et al., 2005), with an overall higher expression on the right side of the heart compared to the left (Figure 3B) (Luo et al., 2008).

To determine the transcript levels of *CRE11*, we used several strand-specific oligonucleotide sets on both sides of the CRE (Figure S3). We found that *CRE11* ncRNA is polyadenylated and transcribed in a bidirectional manner directed away from the element core. However, transcript levels exhibited a unidirectional preference in the direction away from *Kcnh2* (Figure S3). Transcription of ncRNA emerging from CREs occurs at CREs that are actively engaged in gene activation (Kim et al., 2010). Hence CRE tissue specificity is reflected by tissue specificity of the ncRNA transcript. Rather unexpectedly, the transcript levels of *CRE11* ncRNA were in the same range as those of *Kcnh2* mRNA (Figure 3C). Again, we found high transcript levels in cerebellum and cardiac compartments. High expression of *CRE11* was also found in thymus, kidney, and small intestine, whereas the expression of both *Kcnh2* isoforms in these tissues was low (Figures 3B and 3C). Overlay of ChIP-seq datasets for p300, Pol2, and enhancer-associated histone marks in different tissue types revealed that CRE11 is occupied by these proteins in nearly every tissue (Figure S2B), providing a possible explanation for the abundant expression of its ncRNA. Together, these data reveal that *CRE11* ncRNA is strongly transcribed in the murine heart and other organs and suggest a potential role in the transcriptional regulation of *Kcnh2* or nearby genes, either by modulating CRE11 enhancer activity or directly influencing transcriptional regulation.

CRE11 ncRNA Is Involved in the Transcription of *Nos3*, *Abcb8*, and *Kcnh2b* in HL-1 Cell Culture

To test whether the *CRE11* transcript is involved in the regulation of expression of *Kcnh2* or other genes within the TAD, we used antisense oligonucleotides (LNA GapmeRs) to selectively degrade *CRE11* ncRNA in HL-1 cells (Claycomb et al., 1998), which expresses both *Kcnh2a* and *Kcnh2b* and the *CRE11*-derived transcript. Two independent GapmeRs induced an incomplete but reproducible ~50% knockdown of *CRE11* ncRNA at a concentration of 50 nM compared with a scrambled

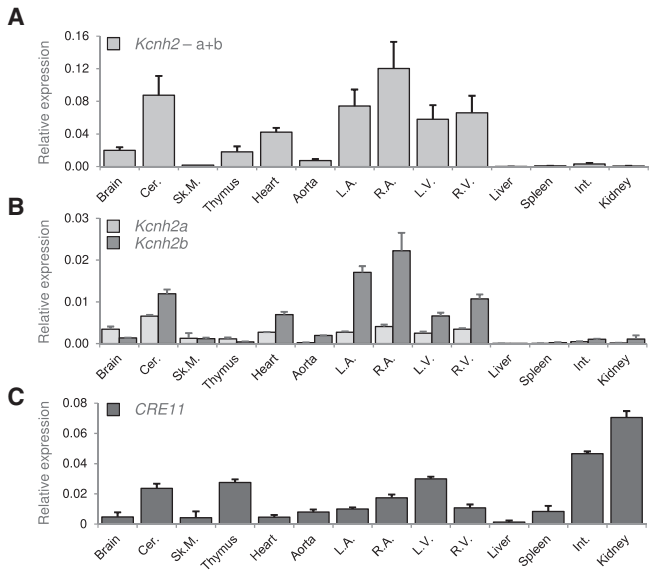

Figure 3. Expression Analysis of *Kcnh2* Isoforms and CRE11 in Murine Adult Tissue Panels

(A) Expression analysis of combined *Kcnh2* isoforms shows that *Kcnh2* is predominantly expressed in brain and heart.

(B) Separated expression analysis of *Kcnh2a* and *Kcnh2b* reveals that *Kcnh2b* is expressed mainly in cardiac tissue and cerebellum, whereas *Kcnh2a* is present at lower levels in multiple tissues.

(C) *CRE11* is expressed in multiple different tissue types. The level of expression of *CRE11* in brain and cardiac compartments corresponds to the expression of *Kcnh2*, but *CRE11* is strongly expressed in intestine and kidney, whereas expression of *Kcnh2* in those tissues is low. Expression levels are normalized to housekeeping gene *Eef2* (Kouadjo et al., 2007).

Error bars represent SD. Cer, cerebellum; Int., intestine; L.A., left atrium; L.V., left ventricle; R.A., right atrium; R.V., right ventricle; Sk.M., skeletal muscle.

control GapmeR (Figure 4A). The expression of *CRE10* ncRNA, transcribed from CRE10 and expressed 100- to 1,000-fold lower compared with *Kcnh2*, was decreased upon knockdown of *CRE11*, suggesting that *CRE10* and *CRE11* function may be coupled or interdependent (Figure 4B). Next, we assessed the effect of knockdown of *CRE11* on all 22 mRNA transcripts within the TAD. Although multiple genes within the TAD physically interact with CRE11, the effect was almost exclusively limited to the genes that displayed a cardiac-enriched interaction with CRE11. We found a significant reduction of the cardiac-enriched isoform *Kcnh2b*, whereas the expression of the more broadly expressed isoform *Kcnh2a* was not affected (Figure 4C). Expression of the neighboring genes *Nos3* and *Abcb8* was also downregulated (Figure 4C), whereas the expression of the other genes within the TAD was unaffected (Figure S4). Heterologously expressed *Kcnh2a* and *Kcnh2b* in HEK293T cells, which do not express either isoform endogenously, were not affected upon transfection of both GapmeRs (Figures S4A and S4B), indicating absence of off-target effects on transcripts of both isoforms as a cause for the observed knockdown. These results suggest that *CRE11* ncRNA could be involved in the expression of *Kcnh2b*, *Nos3*, and *Abcb8*, either by directly controlling their expression or by modulating enhancer function of CRE11.

CRISPR/Cas9-Mediated Deletion of CRE11 in the Mouse Genome Results in Modest Reduction of *Kcnh2* Expression in the Ventricles

To examine the potential role of CRE11 on *Kcnh2* expression *in vivo*, we used CRISPR/Cas9-mediated genome editing to delete the 795 bp CRE11 region (ΔCRE11; Figure 5A; Figure S3). Although targeted homozygous mutations affecting *Kcnh2* causes embryonic lethality with developmental cardiac defects, including affected cardiac looping and outflow tract and branchial arch morphogenesis (Teng et al., 2008), CRE11$^{-/-}$ mice are viable and born according to Mendelian ratios. Analysis of embryonic morphology in wild-type versus homozygous mice did not reveal any affected (cardiac) morphology (data not shown).

Next, we micro-dissected atria, ventricles, and other tissues expressing *Kcnh2* or *CRE11* (brain, intestine, kidney, and liver; Figure 5B; Carrisoza et al., 2010; Farrelly et al., 2003; Huffaker et al., 2009) from CRE11$^{+/+}$ and CRE11$^{-/-}$ E17.5 fetuses and measured expression levels of *Kcnh2a*, *Kcnh2b*, and *CRE11* by qPCR. The expression of *Kcnh2a* was significantly decreased in CRE11$^{-/-}$ fetal ventricles, but not in the atria, compared with wild-type littermates ($p = 0.047$; $n = 11$ and $n = 10$, respectively; Figure 5C). Similarly, the expression of *Kcnh2b* was significantly decreased in fetal ventricles ($p = 0.010$; Figure 5C). Expression of *Kcnh2a* and *Kcnh2b* in other tissues was not significantly changed in CRE11$^{-/-}$ fetuses (Figure 5C). As GapmeR-mediated knockdown of *CRE11* ncRNA results in knockdown of not only *Kcnh2b* but also *Nos3* and *Abcb8* in HL-1 cell culture, and because both ncRNA transcripts and CREs can exert their function on distal genomic regions, we assessed expression levels for all genes within the TAD in fetal CRE11$^{+/+}$ and CRE11$^{-/-}$ ventricles. Deletion of CRE11 did not affect the expression of any of these genes, including *Nos3* and *Abcb8* (Figure 5D). We performed chromosome conformation capture (3C) in adult CRE11$^{+/+}$ and CRE11$^{-/-}$ hearts using the Kcnh2a or Kcnh2b promoter as viewpoint. The results suggest that genomic deletion of CRE11 does not affect the overall topology of the *Kcnh2* locus (Figure S5). Combined, these results show that CRE11 is exclusively involved in but not solely responsible for the cardiac expression of *Kcnh2 in vivo.*

DISCUSSION

The potassium channel encoding gene *KCNH2* is an important regulator of repolarization in the human heart, yet little is known about its transcriptional regulation. Several genome-wide association studies have implicated non-coding variants in the *KCNH2* locus in humans with QT interval duration (Arking et al., 2014; Méndez-Giráldez et al., 2017; Newton-Cheh et al., 2009; Pfeufer et al., 2009), suggesting that perturbations in non-coding regulatory sequences driving its expression can affect *KCNH2* regulation and function. In this study, we aimed to elucidate the regulatory mechanisms underlying *Kcnh2* expression. We identified an active regulatory element (CRE11) that is in close physical proximity to *Kcnh2* in the heart, drives transgene expression in transient transfection assays and zebrafish heart, and produces a ncRNA that is involved in the expression of *Kcnh2b* but not *Kcnh2a* in HL-1 cells. Deletion of

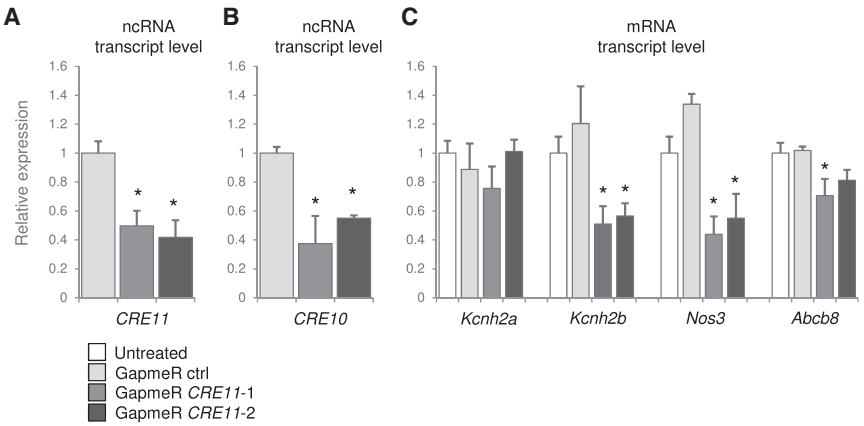

Figure 4. Functional Knockdown of *CRE11* in HL-1 Cells Results in Reduced Expression of *CRE10*, *Kcnh2b*, *Nos3*, and *Abcb8*

(A) qPCR analysis of *CRE11* after knockdown with two independent GapmeRs shows a consistent 50% reduction in ncRNA expression.

(B) Knockdown of *CRE11* causes reduced expression level of the ncRNA transcript derived from the neighboring CRE10 region.

(C) A significant reduction in expression is observed for *Kcnh2b*, *Nos3*, and *Abcb8* upon *CRE11* knockdown with two separate GapmeRs. Data are normalized to the scrambled GapmeR control.

Error bars represent SD. *$p < 0.05$. See also Figures S2B, S3, and S4.

endogenous CRE11 causes only a slight but significant reduction of expression levels *in vivo* of both *Kcnh2* isoforms in fetal ventricles and does not affect atrial expression. Recently, multiple studies have demonstrated that regulatory sequences capable of driving gene expression often act in a redundant manner and that genomic deletion of individual enhancer regions does not necessarily recapitulate the phenotype that is observed in full knockouts of the target gene (Cunningham et al., 2018; Osterwalder et al., 2018; Sarro et al., 2018). The small decrease in gene expression we observe in CRE11$^{-/-}$ hearts therefore suggests that other REs within the TAD besides CRE11 are involved in the regulation of *Kcnh2* expression. Genomic deletion of CRE11 did not, however, result in increased contact between either promoter with the various tested regions within the locus, including several putative CREs. This suggests that novel or increased contacts do not appear upon deletion of CRE11 or, alternatively, that deletion of CRE11 does not rewire the three dimensional topology of the *Kcnh2* locus. Nevertheless, our 3C results do not exclude the possibility that other regions increase or decrease their contact frequency with *Kcnh2a* or *Kcnh2b* upon deletion of CRE11. Our *in vitro* analysis indicates that among others CRE7 and CRE9 hold regulatory potential and physically contact *Kcnh2*, setting the stage for a potential regulatory function individually or in synergy with CRE11 and thereby providing robustness to the regulatory complex in conditions of impaired RE function.

Selective but incomplete knockdown of *CRE11* ncRNA in HL-1 cells resulted in a significant downregulation of *Kcnh2b* but not of the more broadly expressed *Kcnh2a*, suggestive of a cardiac-specific function of both *CRE11* and *Kcnh2b*. Accordingly, a recent study showed that deletion of *NKX2-5*, encoding a transcription factor crucial for cardiac development, results in impaired cardiomyogenesis and knockdown of *Kcnh2b* but not of *Kcnh2a* in human embryonic stem cells (Anderson et al., 2018). *Kcnh2b* encodes Merg1b, the murine equivalent of the human hERG1b. In both human and mouse, it co-assembles with the 1a subunit to form heteromeric K^+-selective channels with properties similar to the rapidly activating component of the delayed rectifier K^+ current (I_{Kr}) (Holzem et al., 2016; Jones et al., 2004; Larsen et al., 2008; London et al., 1997). hERG1a has long been regarded as the critical component of cardiac repolarization, whereas the contribution of hERG1b in the human heart has been disputed (Larsen et al., 2008; Pond and Nerbonne, 2001). However, repolarization of the cardiac action potential has been demonstrated to be mediated by heteromeric hERG channels, rather than homomeric channels. Knockdown of the 1b subunit in induced pluripotent stem cell-derived cardiomyocytes (iPSC-CMs) resulted in reduced *KCNH2B* expression and peak-tail I_{Kr} density (Jones et al., 2014), and clinically identified mutations in hERG1b lead to LQTS type 2 (Crotti et al., 2013; Sale et al., 2008). When placed in the perspective of our present study, this entails that a specific downregulation of only *Kcnh2b* by loss of *CRE11* can lead to affected expression and function of *KCNH2*. Furthermore, our results show that knockdown of *CRE11* in HL-1 cells does not solely affect the expression of *Kcnh2b* but also reduces the expression of *Nos3* and *Abcb8*, two genes upstream of *Kcnh2* within the same TAD. Both *NOS3* and *ABCB8* have been associated with heart failure (HF), and their expression is downregulated in hearts of patients with end-stage HF (Ichikawa et al., 2012; Piech et al., 2002). *Nos3*$^{-/-}$ mice show extensive ventricular remodeling, hypertrophy, and contractile dysfunction after myocardial infarction (Scherrer-Crosbie et al., 2001), whereas targeted knockdown of *Abcb8* in mice results in mitochondrial iron accumulation, increased cell death, and cardiomyopathy (Ichikawa et al., 2012). The closely related function of *KCNH2B*, *NOS3*, and *ABCB8* in cardiac function and their response to *CRE11* knockdown in cell culture suggests a regulatory network in which *CRE11* ncRNA coordinates the expression of *Kcnh2b*, *Nos3*, and *Abcb8 in vivo.* The unaffected expression of *Nos3* and *Abcb8* and the minor decrease in expression of *Kcnh2b* upon deletion of endogenous CRE11 *in vivo*, however, reveals a discrepancy between *CRE11* transcript knockdown and deletion of the underlying endogenous CRE11 sequence. This suggests a mechanism whereby *CRE11* ncRNA regulates cardiac-specific expression of only the *Kcnh2b* isoform (and *Nos3* and *Abcb8*), whereas the underlying genomic element CRE11 is involved in more general cardiac expression of both *Kcnh2a* and *Kcnh2b* but not of *Nos3* and *Abcb8*. *CRE11* ncRNA could function by maintaining CRE11 function and stability, as shown for other enhancer RNAs (Kopp and Mendell, 2018; Rothschild and Basu, 2017). Its knockdown then possibly causes misregulation

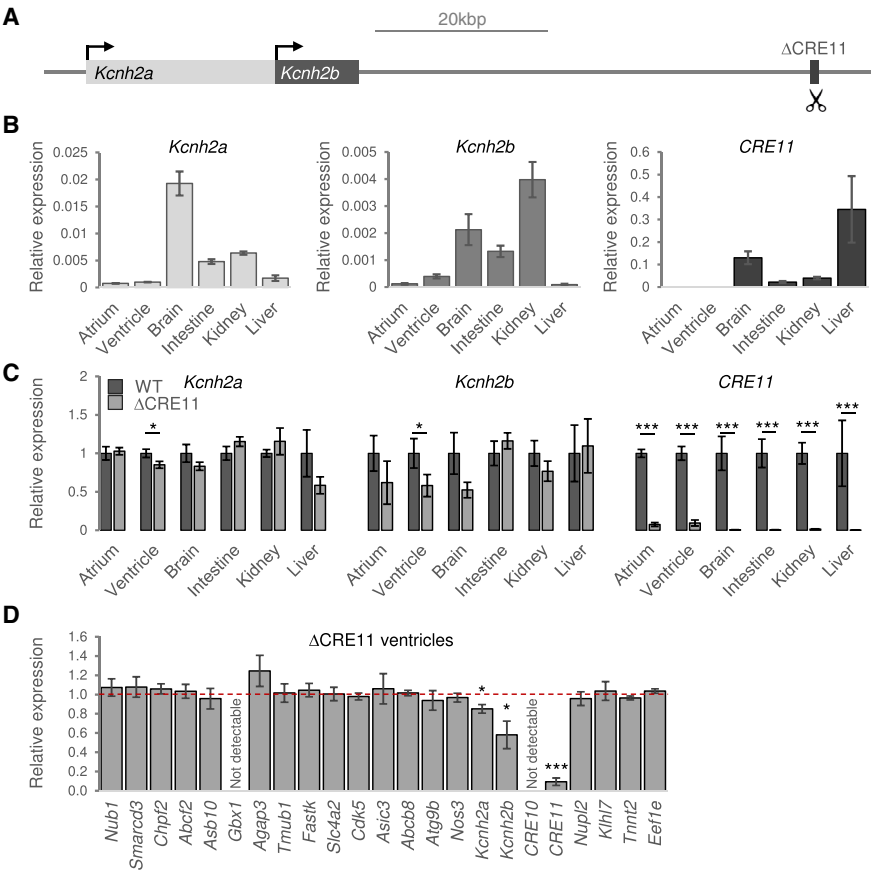

Figure 5. Genomic Deletion of *CRE11* by CRISPR/Cas9-Mediated Genome Editing Affects Fetal Ventricular *Kcnh2* Expression

(A) Schematic overview of the murine *Kcnh2* locus with the location of *Kcnh2a*, *Kcnh2b*, and the deleted CRE11 site.

(B) Expression levels of *Kcnh2a*, *Kcnh2b*, and *CRE11* in wild-type fetal (E17.5) tissues.

(C) Expression levels of *Kcnh2a*, *Kcnh2b*, and *CRE11* in CRE11$^{+/+}$ and CRE11$^{-/-}$ fetal tissues. Values are depicted as normalized expression of mutant versus wild-type expression levels.

(D) Expression of *Kcnh2b* in genes within the *Kcnh2* TAD in CRE11$^{-/-}$ fetal ventricles. Values are depicted as normalized expression of mutant versus wild-type expression levels. Expression levels are normalized to *Eef2*. CRE11$^{+/+}$ (wild-type), n = 11; CRE11$^{-/-}$ (mutant), n = 10.

Error bars represent SD. *p < 0.05 and ***p < 0.01. See also Figures S4 and S5.

of CRE11 and, consequently, of *Kcnh2b*, *Nos3*, or *Abcb8*. Although speculative, the discrepancy between a potential role of *CRE11* ncRNA in *Nos3* and *Abcb8* expression and the unaffected expression of *Nos3* and *Abcb8* upon deletion of endogenous CRE11 might be caused by compensatory mechanisms, possibly through the activity of additional regulatory sequences, that buffer the loss of CRE11 and its associated ncRNA throughout development. As we limited our investigations of the effects of *CRE11* to genes within 1 Mb of its location of origin on the basis of the TAD, our results do not exclude the possibility of a *trans*-acting role of the *CRE11* ncRNA on the expression of more distantly located genes. Analysis of the effects of *CRE11* ncRNA on a genome-wide scale by RNA sequencing of cardiac tissue of CRE11$^{-/-}$ mice could elucidate the full potential of this CRE or its derived ncRNA.

Previous work showed that knockdown of *Kcnh2b* but not *Kcnh2a* in mice eliminates I_{Kr} from both fetal and adult ventricular cardiomyocytes and results in episodic sinus bradycardia but not QT prolongation (Lees-Miller et al., 2003). Knockout of all *Kcnh2* isoforms leads to embryonic lethality and a failure of the heart and brain to develop normally (London et al., 1997; Teng et al., 2008). In the present study, we measured expression levels in fetal atrial and ventricular cells from Kcnh2-CRE11$^{+/+}$ and Kcnh2-CRE11$^{-/-}$ mice to assess the role of CRE11 *in vivo*. As deletion of CRE11 only lead to a small decrease of *Kcnh2* expression in fetal ventricles, we did not expect significant or measurable functional effects on mERG1 channel expression or function, and as such we did not evaluate electrophysiological parameters. Furthermore, although *KCNH2* is a major contributor to the I_{Kr} current responsible for myocardial repolarization in the human heart, repolarization in murine cardiomyocytes is much faster and mediated by other currents (Brouillette et al., 2004; Guo et al., 1999; Xu et al., 1999), and the role of I_{Kr} is negligible (Xu et al., 1999). With this study, we therefore predominantly aimed to understand the mechanisms underlying the transcriptional regulation of *Kcnh2* and its isoforms rather than to elucidate the functional effects of disrupted regulation on ion channel function *in vivo*. Nevertheless, our results do not exclude the possibility that expression or function of *Kcnh2* or other genes within the TAD might be affected in other tissues or conditions.

Common single-nucleotide polymorphisms (SNPs) affecting QT interval duration have been identified within the *KCNH2* locus by genome-wide association study (GWAS) (Arking et al., 2014; Newton-Cheh et al., 2009; Pfeufer et al., 2009), functionally implicating non-coding DNA surrounding *KCNH2* with cardiac repolarization. Altered transcription factor binding through common variants has been linked to affected regulation of several cardiac genes (Beaudoin et al., 2015; Kapoor et al., 2014; Reschen et al., 2015; Smemo et al., 2012), including LQTS genes *SCN5A* (van den Boogaard et al., 2014) and *KCNQ1* (Amin et al., 2012). Except for a variant within CRE10 (rs9640171; Arking et al., 2014), LQTS variants identified through GWAS (Arking et al., 2014; Newton-Cheh et al., 2009; Pfeufer et al., 2009), including variants in linkage disequilibrium, do not overlap putative CREs in the *KCNH2* locus (Figure S1). Although *CRE10* transcript is decreased upon *CRE11* knockdown in HL-1 cells and therefore possibly involved in *Kcnh2* regulation, we did not observe any regulatory activity of CRE10 *in vitro* in

multiple cell lines or *in vivo* in transgenic zebrafish reporter assays and therefore did not pursue potential effects on gene expression caused by this variant. GWAS associations can arise from multiple variants within a locus that together, but not necessarily individually, implicate loci to traits (Cannon and Mohlke, 2018; Chatterjee et al., 2016). The variant within CRE10 or other variants within the locus could thus still affect the regulatory network driving *Kcnh2* expression *in vivo* in manners that are undetectable by the experimental procedures as used in this study. In contrast to common variation identified through GWAS, rare variants overlapping CREs could theoretically still be identified through disease-specific studies, but these are difficult for relatively uncommon diseases such as LQTS. The likelihood of rare non-coding variants contributing to a common cause for LQTS is small, but examples have been published in other fields of research (Duan et al., 2014; Lee et al., 2014). Combined, our results increase our knowledge of the mechanisms underlying the complex regulation of *KCNH2*, which provides important information in the prediction of LQTS susceptibility and progression in patients.

STAR★METHODS

Detailed methods are provided in the online version of this paper and include the following:

- KEY RESOURCES TABLE
- LEAD CONTACT AND MATERIALS AVAILABILITY
- EXPERIMENTAL MODEL AND SUBJECT DETAILS
  - Cell Lines and Culture Conditions
  - Animals and *In Vivo* Procedures
  - Study Approval
- METHOD DETAILS
  - Identification of putative REs
  - Cloning, Transfection and Luciferase assays
  - *In vivo* zebrafish assay
  - Preparation of 4C-template
  - 4C-seq primer design
  - 4C data analysis and statistics
  - Quantitative expression analysis
  - Knockdown experiments using LNA^{TM} GapmeRs
  - Generation of mutant mice
  - Chromosome Conformation Capture (3C)
- QUANTIFICATION AND STATISTICAL ANALYSIS
- DATA AND CODE AVAILABILITY

SUPPLEMENTAL INFORMATION

Supplemental Information can be found online at https://doi.org/10.1016/j.celrep.2019.08.007.

ACKNOWLEDGMENTS

We thank Vincent Wakker, Jan M. Ruijter, and Sonja Chocron for their contributions. This work was supported by the Netherlands Cardiovascular Research Initiative (CVON) HUSTCARE project; Fondation Leducq (14CVD01); and the European Community's Seventh Framework Programme contract (CardioGeNet, 223463).

AUTHOR CONTRIBUTIONS

M.v.d.B., J.H.v.W., V.M.C., and P.B. developed the experimental design. M.v.d.B., J.H.v.W., and A.C.B. performed most of the experiments. I.B.H. and F.T. performed the zebrafish experiments. H.J.G.v.d.W. and W.d.L. facilitated the 4C sequencing experiments. H.J.G.v.d.W. analyzed the 4C sequencing data. M.v.d.B., J.H.v.W., and V.M.C. wrote the paper. All authors edited the paper. V.M.C., P.B., W.L., and J.B. supervised the work. This work was part of M.v.d.B.'s thesis research as a PhD student at the University of Amsterdam.

DECLARATION OF INTERESTS

The authors declare no competing interests.

Received: November 8, 2018
Revised: June 5, 2019
Accepted: July 30, 2019
Published: September 3, 2019

REFERENCES

Amin, A.S., Giudicessi, J.R., Tijsen, A.J., Spanjaart, A.M., Reckman, Y.J., Klemens, C.A., Tanck, M.W., Kapplinger, J.D., Hofman, N., Sinner, M.F., et al. (2012). Variants in the 3′ untranslated region of the KCNQ1-encoded Kv7.1 potassium channel modify disease severity in patients with type 1 long QT syndrome in an allele-specific manner. Eur. Heart J. *33*, 714–723.

Anderson, D.J., Kaplan, D.I., Bell, K.M., Koutsis, K., Haynes, J.M., Mills, R.J., Phelan, D.G., Qian, E.L., Leitoguinho, A.R., Arasaratnam, D., et al. (2018). NKX2-5 regulates human cardiomyogenesis via a HEY2 dependent transcriptional network. Nat. Commun. *9*, 1373.

Andersson, R., Gebhard, C., Miguel-Escalada, I., Hoof, I., Bornholdt, J., Boyd, M., Chen, Y., Zhao, X., Schmidl, C., Suzuki, T., et al. (2014). An atlas of active enhancers across human cell types and tissues. Nature *507*, 455–461.

Andrey, G., and Mundlos, S. (2017). The three-dimensional genome: regulating gene expression during pluripotency and development. Development *144*, 3646–3658.

Archer, K., Broskova, Z., Bayoumi, A.S., Teoh, J.P., Davila, A., Tang, Y., Su, H., and Kim, I.M. (2015). Long non-coding RNAs as master regulators in cardiovascular diseases. Int. J. Mol. Sci. *16*, 23651–23667.

Arking, D.E., Pulit, S.L., Crotti, L., van der Harst, P., Munroe, P.B., Koopmann, T.T., Sotoodehnia, N., Rossin, E.J., Morley, M., Wang, X., et al.; CARe Consortium; COGENT Consortium; DCCT/EDIC; eMERGE Consortium; HRGEN Consortium (2014). Genetic association study of QT interval highlights role for calcium signaling pathways in myocardial repolarization. Nat. Genet. *46*, 826–836.

Arner, E., Daub, C.O., Vitting-Seerup, K., Andersson, R., Lilje, B., Drabløs, F., Lennartsson, A., Rönnerblad, M., Hrydziuszko, O., Vitezic, M., et al.; FANTOM Consortium (2015). Transcribed enhancers lead waves of coordinated transcription in transitioning mammalian cells. Science *347*, 1010–1014.

Barski, A., Cuddapah, S., Cui, K., Roh, T.Y., Schones, D.E., Wang, Z., Wei, G., Chepelev, I., and Zhao, K. (2007). High-resolution profiling of histone methylations in the human genome. Cell *129*, 823–837.

Beaudoin, M., Gupta, R.M., Won, H.H., Lo, K.S., Do, R., Henderson, C.A., Lavoie-St-Amour, C., Langlois, S., Rivas, D., Lehoux, S., et al. (2015). Myocardial infarction-associated SNP at 6p24 interferes with MEF2 binding and associates with PHACTR1 expression levels in human coronary arteries. Arterioscler. Thromb. Vasc. Biol. *35*, 1472–1479.

Bessa, J., Tena, J.J., de la Calle-Mustienes, E., Fernández-Miñán, A., Naranjo, S., Fernández, A., Montoliu, L., Akalin, A., Lenhard, B., Casares, F., and Gómez-Skarmeta, J.L. (2009). Zebrafish enhancer detection (ZED) vector: a new tool to facilitate transgenesis and the functional analysis of cis-regulatory regions in zebrafish. Dev. Dyn. *238*, 2409–2417.

Boogerd, C.J., Zhu, X., Aneas, I., Sakabe, N.J., Zhang, L., Sobreira, D.R., Montefiori, L.E., Bogomolovas, J., Joslin, A.C., Zhou, B., et al. (2018). Tbx20

is required in mid-gestation cardiomyocytes and plays a central role in atrial development. Circ. Res. *123*, 428–442.

Boon, R.A., Jaé, N., Holdt, L., and Dimmeler, S. (2016). Long noncoding RNAs: from clinical genetics to therapeutic targets? J. Am. Coll. Cardiol. *67*, 1214–1226.

Brouillette, J., Clark, R.B., Giles, W.R., and Fiset, C. (2004). Functional properties of K+ currents in adult mouse ventricular myocytes. J. Physiol. *559*, 777–798.

Caballero, R., Utrilla, R.G., Amorós, I., Matamoros, M., Pérez-Hernández, M., Tinaquero, D., Alfayate, S., Nieto-Marín, P., Guerrero-Serna, G., Liu, Q.H., et al. (2017). Tbx20 controls the expression of the KCNH2 gene and of hERG channels. Proc. Natl. Acad. Sci. U S A *114*, E416–E425.

Cannon, M.E., and Mohlke, K.L. (2018). Deciphering the emerging complexities of molecular mechanisms at GWAS loci. Am. J. Hum. Genet. *103*, 637–653.

Carrisoza, R., Salvador, C., Bobadilla, N.A., Trujillo, J., and Escobar, L.I. (2010). Expression and immunolocalization of ERG1 potassium channels in the rat kidney. Histochem. Cell Biol. *133*, 189–199.

Chatterjee, S., Kapoor, A., Akiyama, J.A., Auer, D.R., Lee, D., Gabriel, S., Berrios, C., Pennacchio, L.A., and Chakravarti, A. (2016). Enhancer variants synergistically drive dysfunction of a gene regulatory network in Hirschsprung disease. Cell *167*, 355–368.e10.

Cheng, C.F., Kuo, T.B., Chen, W.N., Lin, C.C., and Chen, C.C. (2014). Abnormal cardiac autonomic regulation in mice lacking ASIC3. BioMed Res. Int. *2014*, 709159.

Claycomb, W.C., Lanson, N.A., Jr., Stallworth, B.S., Egeland, D.B., Delcarpio, J.B., Bahinski, A., and Izzo, N.J., Jr. (1998). HL-1 cells: a cardiac muscle cell line that contracts and retains phenotypic characteristics of the adult cardiomyocyte. Proc. Natl. Acad. Sci. U S A *95*, 2979–2984.

Clouaire, T., Webb, S., Skene, P., Illingworth, R., Kerr, A., Andrews, R., Lee, J.H., Skalnik, D., and Bird, A. (2012). Cfp1 integrates both CpG content and gene activity for accurate H3K4me3 deposition in embryonic stem cells. Genes Dev. *26*, 1714–1728.

Cong, L., Ran, F.A., Cox, D., Lin, S., Barretto, R., Habib, N., Hsu, P.D., Wu, X., Jiang, W., Marraffini, L.A., and Zhang, F. (2013). Multiplex genome engineering using CRISPR/Cas systems. Science *339*, 819–823.

ENCODE Project Consortium (2012). An integrated encyclopedia of DNA elements in the human genome. Nature *489*, 57–74.

Crotti, L., Tester, D.J., White, W.M., Bartos, D.C., Insolia, R., Besana, A., Kunic, J.D., Will, M.L., Velasco, E.J., Bair, J.J., et al. (2013). Long QT syndrome-associated mutations in intrauterine fetal death. JAMA *309*, 1473–1482.

Cunningham, T.J., Lancman, J.J., Berenguer, M., Dong, P.D.S., and Duester, G. (2018). Genomic knockout of two presumed forelimb Tbx5 enhancers reveals they are nonessential for limb development. Cell Rep. *23*, 3146–3151.

de Boer, B.A., van Duijvenboden, K., van den Boogaard, M., Christoffels, V.M., Barnett, P., and Ruijter, J.M. (2014). OccuPeak: ChIP-seq peak calling based on internal background modelling. PLoS ONE *9*, e99844.

de Castro, M.P., Aránega, A., and Franco, D. (2006). Protein distribution of Kcnq1, Kcnh2, and Kcne3 potassium channel subunits during mouse embryonic development. Anat. Rec. A Discov. Mol. Cell. Evol. Biol. *288*, 304–315.

de Laat, W., and Duboule, D. (2013). Topology of mammalian developmental enhancers and their regulatory landscapes. Nature *502*, 499–506.

De Santa, F., Barozzi, I., Mietton, F., Ghisletti, S., Polletti, S., Tusi, B.K., Muller, H., Ragoussis, J., Wei, C.L., and Natoli, G. (2010). A large fraction of extragenic RNA pol II transcription sites overlap enhancers. PLoS Biol. *8*, e1000384.

Duan, J., Shi, J., Fiorentino, A., Leites, C., Chen, X., Moy, W., Chen, J., Alexandrov, B.S., Usheva, A., He, D., et al.; Molecular Genetics of Schizophrenia collaboration; Genomic Psychiatric Cohort consortium (2014). A rare functional noncoding variant at the GWAS-implicated MIR137/MIR2682 locus might confer risk to schizophrenia and bipolar disorder. Am. J. Hum. Genet. *95*, 744–753.

Farrelly, A.M., Ro, S., Callaghan, B.P., Khoyi, M.A., Fleming, N., Horowitz, B., Sanders, K.M., and Keef, K.D. (2003). Expression and function of KCNH2 (HERG) in the human jejunum. Am. J. Physiol. Gastrointest. Liver Physiol. *284*, G883–G895.

Ghirlando, R., and Felsenfeld, G. (2016). CTCF: making the right connections. Genes Dev. *30*, 881–891.

Giudicessi, J.R., and Ackerman, M.J. (2013). Determinants of incomplete penetrance and variable expressivity in heritable cardiac arrhythmia syndromes. Transl. Res. *161*, 1–14.

Gong, Q., Stump, M.R., and Zhou, Z. (2014). Upregulation of functional Kv11.1 isoform expression by inhibition of intronic polyadenylation with antisense morpholino oligonucleotides. J. Mol. Cell. Cardiol. *76*, 26–32.

Guasti, L., Crociani, O., Redaelli, E., Pillozzi, S., Polvani, S., Masselli, M., Mello, T., Galli, A., Amedei, A., Wymore, R.S., et al. (2008). Identification of a post-translational mechanism for the regulation of hERG1 K+ channel expression and hERG1 current density in tumor cells. Mol. Cell. Biol. *28*, 5043–5060.

Guo, W., Xu, H., London, B., and Nerbonne, J.M. (1999). Molecular basis of transient outward K+ current diversity in mouse ventricular myocytes. J. Physiol. *521*, 587–599.

Hagège, H., Klous, P., Braem, C., Splinter, E., Dekker, J., Cathala, G., de Laat, W., and Forné, T. (2007). Quantitative analysis of chromosome conformation capture assays (3C-qPCR). Nat. Protoc. *2*, 1722–1733.

Heintzman, N.D., Stuart, R.K., Hon, G., Fu, Y., Ching, C.W., Hawkins, R.D., Barrera, L.O., Van Calcar, S., Qu, C., Ching, K.A., et al. (2007). Distinct and predictive chromatin signatures of transcriptional promoters and enhancers in the human genome. Nat. Genet. *39*, 311–318.

Hofmann, P., and Boon, R.A. (2014). Non-coding RNA enhances cardiac development. J. Mol. Cell. Cardiol. *76*, 205–207.

Holwerda, S.J., and de Laat, W. (2013). CTCF: the protein, the binding partners, the binding sites and their chromatin loops. Philos. Trans. R. Soc. Lond. B Biol. Sci. *368*, 20120369.

Holzem, K.M., Gomez, J.F., Glukhov, A.V., Madden, E.J., Koppel, A.C., Ewald, G.A., Trenor, B., and Efimov, I.R. (2016). Reduced response to IKr blockade and altered hERG1a/1b stoichiometry in human heart failure. J. Mol. Cell. Cardiol. *96*, 82–92.

Huffaker, S.J., Chen, J., Nicodemus, K.K., Sambataro, F., Yang, F., Mattay, V., Lipska, B.K., Hyde, T.M., Song, J., Rujescu, D., et al. (2009). A primate-specific, brain isoform of KCNH2 affects cortical physiology, cognition, neuronal repolarization and risk of schizophrenia. Nat. Med. *15*, 509–518.

Ichikawa, Y., Bayeva, M., Ghanefar, M., Potini, V., Sun, L., Mutharasan, R.K., Wu, R., Khechaduri, A., Jairaj Naik, T., and Ardehali, H. (2012). Disruption of ATP-binding cassette B8 in mice leads to cardiomyopathy through a decrease in mitochondrial iron export. Proc. Natl. Acad. Sci. U S A *109*, 4152–4157.

Jones, E.M., Roti Roti, E.C., Wang, J., Delfosse, S.A., and Robertson, G.A. (2004). Cardiac IKr channels minimally comprise hERG 1a and 1b subunits. J. Biol. Chem. *279*, 44690–44694.

Jones, D.K., Liu, F., Vaidyanathan, R., Eckhardt, L.L., Trudeau, M.C., and Robertson, G.A. (2014). hERG 1b is critical for human cardiac repolarization. Proc. Natl. Acad. Sci. U S A *111*, 18073–18077.

Kapoor, A., Sekar, R.B., Hansen, N.F., Fox-Talbot, K., Morley, M., Pihur, V., Chatterjee, S., Brandimarto, J., Moravec, C.S., Pulit, S.L., et al.; QT Interval-International GWAS Consortium (2014). An enhancer polymorphism at the cardiomyocyte intercalated disc protein NOS1AP locus is a major regulator of the QT interval. Am. J. Hum. Genet. *94*, 854–869.

Kim, T.K., Hemberg, M., Gray, J.M., Costa, A.M., Bear, D.M., Wu, J., Harmin, D.A., Laptewicz, M., Barbara-Haley, K., Kuersten, S., et al. (2010). Widespread transcription at neuronal activity-regulated enhancers. Nature *465*, 182–187.

Kopp, F., and Mendell, J.T. (2018). Functional classification and experimental dissection of long noncoding RNAs. Cell *172*, 393–407.

Kouadjo, K.E., Nishida, Y., Cadrin-Girard, J.F., Yoshioka, M., and St-Amand, J. (2007). Housekeeping and tissue-specific genes in mouse tissues. BMC Genomics *8*, 127.

Kupershmidt, S., Snyders, D.J., Raes, A., and Roden, D.M. (1998). A K+ channel splice variant common in human heart lacks a C-terminal domain required

for expression of rapidly activating delayed rectifier current. J. Biol. Chem. *273*, 27231–27235.

Kwan, K.M., Fujimoto, E., Grabher, C., Mangum, B.D., Hardy, M.E., Campbell, D.S., Parant, J.M., Yost, H.J., Kanki, J.P., and Chein, C.B. (2007). The Tol2kit: A multisite gateway-based construction kit for *Tol2* transposon transgenesis constructs. Dev. Dyn. *236*, 3088–3099.

Larsen, A.P., Olesen, S.P., Grunnet, M., and Jespersen, T. (2008). Characterization of hERG1a and hERG1b potassium channels-a possible role for hERG1b in the I (Kr) current. Pflugers Arch. *456*, 1137–1148.

Lauberth, S.M., Nakayama, T., Wu, X., Ferris, A.L., Tang, Z., Hughes, S.H., and Roeder, R.G. (2013). H3K4me3 interactions with TAF3 regulate preinitiation complex assembly and selective gene activation. Cell *152*, 1021–1036.

Lee, S., Abecasis, G.R., Boehnke, M., and Lin, X. (2014). Rare-variant association analysis: study designs and statistical tests. Am. J. Hum. Genet. *95*, 5–23.

Lees-Miller, J.P., Kondo, C., Wang, L., and Duff, H.J. (1997). Electrophysiological characterization of an alternatively processed ERG K+ channel in mouse and human hearts. Circ. Res. *81*, 719–726.

Lees-Miller, J.P., Guo, J., Somers, J.R., Roach, D.E., Sheldon, R.S., Rancourt, D.E., and Duff, H.J. (2003). Selective knockout of mouse ERG1 B potassium channel eliminates $I_{(Kr)}$ in adult ventricular myocytes and elicits episodes of abrupt sinus bradycardia. Mol. Cell. Biol. *23*, 1856–1862.

Li, W., Notani, D., Ma, Q., Tanasa, B., Nunez, E., Chen, A.Y., Merkurjev, D., Zhang, J., Ohgi, K., Song, X., et al. (2013). Functional roles of enhancer RNAs for oestrogen-dependent transcriptional activation. Nature *498*, 516–520.

London, B., Trudeau, M.C., Newton, K.P., Beyer, A.K., Copeland, N.G., Gilbert, D.J., Jenkins, N.A., Satler, C.A., and Robertson, G.A. (1997). Two isoforms of the mouse ether-a-go-go-related gene coassemble to form channels with properties similar to the rapidly activating component of the cardiac delayed rectifier K+ current. Circ. Res. *81*, 870–878.

Luo, X., Xiao, J., Lin, H., Lu, Y., Yang, B., and Wang, Z. (2008). Genomic structure, transcriptional control, and tissue distribution of HERG1 and KCNQ1 genes. Am. J. Physiol. Heart Circ. Physiol. *294*, H1371–H1380.

Marionneau, C., Couette, B., Liu, J., Li, H., Mangoni, M.E., Nargeot, J., Lei, M., Escande, D., and Demolombe, S. (2005). Specific pattern of ionic channel gene expression associated with pacemaker activity in the mouse heart. J. Physiol. *562*, 223–234.

Maurano, M.T., Humbert, R., Rynes, E., Thurman, R.E., Haugen, E., Wang, H., Reynolds, A.P., Sandstrom, R., Qu, H., Brody, J., et al. (2012). Systematic localization of common disease-associated variation in regulatory DNA. Science *337*, 1190–1195.

Méndez-Giráldez, R., Gogarten, S.M., Below, J.E., Yao, J., Seyerle, A.A., Highland, H.M., Kooperberg, C., Soliman, E.Z., Rotter, J.I., Kerr, K.F., et al. (2017). GWAS of the electrocardiographic QT interval in Hispanics/Latinos generalizes previously identified loci and identifies population-specific signals. Sci. Rep. *7*, 17075.

Mercer, T.R., Dinger, M.E., and Mattick, J.S. (2009). Long non-coding RNAs: insights into functions. Nat. Rev. Genet. *10*, 155–159.

modENCODE Consortium; Roy, S., Ernst, J., Kharchenko, P.V., Kheradpour, P., Negre, N., Eaton, M.L., Landolin, J.M., Bristow, C.A., Ma, L., et al. (2010). Identification of functional elements and regulatory circuits by Drosophila modENCODE. Science *330*, 1787–1797.

Monroe, T.O., Hill, M.C., Morikawa, Y., Leach, J.P., Heallen, T., Cao, S., Krijger, P.H.L., de Laat, W., Wehrens, X.H.T., Rodney, G.G., and Martin, J.F. (2019). YAP partially reprograms chromatin accessibility to directly induce adult cardiogenesis in vivo. Dev. Cell *48*, 765–779.e7.

Naumova, N., Smith, E.M., Zhan, Y., and Dekker, J. (2012). Analysis of long-range chromatin interactions using chromosome conformation capture. Methods *58*, 192–203.

Newton-Cheh, C., Eijgelsheim, M., Rice, K.M., de Bakker, P.I., Yin, X., Estrada, K., Bis, J.C., Marciante, K., Rivadeneira, F., Noseworthy, P.A., et al. (2009). Common variants at ten loci influence QT interval duration in the QTGEN study. Nat. Genet. *41*, 399–406.

Osterwalder, M., Barozzi, I., Tissières, V., Fukuda-Yuzawa, Y., Mannion, B.J., Afzal, S.Y., Lee, E.A., Zhu, Y., Plajzer-Frick, I., Pickle, C.S., et al. (2018). Enhancer redundancy provides phenotypic robustness in mammalian development. Nature *554*, 239–243.

Pekowska, A., Benoukraf, T., Zacarias-Cabeza, J., Belhocine, M., Koch, F., Holota, H., Imbert, J., Andrau, J.C., Ferrier, P., and Spicuglia, S. (2011). H3K4 tri-methylation provides an epigenetic signature of active enhancers. EMBO J. *30*, 4198–4210.

Pfeufer, A., Sanna, S., Arking, D.E., Müller, M., Gateva, V., Fuchsberger, C., Ehret, G.B., Orrú, M., Pattaro, C., Köttgen, A., et al. (2009). Common variants at ten loci modulate the QT interval duration in the QTSCD study. Nat. Genet. *41*, 407–414.

Piech, A., Massart, P.E., Dessy, C., Feron, O., Havaux, X., Morel, N., Vanoverschelde, J.L., Donckier, J., and Balligand, J.L. (2002). Decreased expression of myocardial eNOS and caveolin in dogs with hypertrophic cardiomyopathy. Am. J. Physiol. Heart Circ. Physiol. *282*, H219–H231.

Pond, A.L., and Nerbonne, J.M. (2001). ERG proteins and functional cardiac I(Kr) channels in rat, mouse, and human heart. Trends Cardiovasc. Med. *11*, 286–294.

Rao, S.S., Huntley, M.H., Durand, N.C., Stamenova, E.K., Bochkov, I.D., Robinson, J.T., Sanborn, A.L., Machol, I., Omer, A.D., Lander, E.S., and Aiden, E.L. (2014). A 3D map of the human genome at kilobase resolution reveals principles of chromatin looping. Cell *159*, 1665–1680.

Reschen, M.E., Gaulton, K.J., Lin, D., Soilleux, E.J., Morris, A.J., Smyth, S.S., and O'Callaghan, C.A. (2015). Lipid-induced epigenomic changes in human macrophages identify a coronary artery disease-associated variant that regulates PPAP2B expression through altered C/EBP-beta binding. PLoS Genet. *11*, e1005061.

Rothschild, G., and Basu, U. (2017). Lingering questions about enhancer RNA and enhancer transcription-coupled genomic instability. Trends Genet. *33*, 143–154.

Ruijter, J.M., Ramakers, C., Hoogaars, W.M., Karlen, Y., Bakker, O., van den Hoff, M.J., and Moorman, A.F. (2009). Amplification efficiency: linking baseline and bias in the analysis of quantitative PCR data. Nucleic Acids Res. *37*, e45.

Sale, H., Wang, J., O'Hara, T.J., Tester, D.J., Phartiyal, P., He, J.Q., Rudy, Y., Ackerman, M.J., and Robertson, G.A. (2008). Physiological properties of hERG 1a/1b heteromeric currents and a hERG 1b-specific mutation associated with Long-QT syndrome. Circ. Res. *103*, e81–e95.

Sander, J.D., Maeder, M.L., Reyon, D., Voytas, D.F., Joung, J.K., and Dobbs, D. (2010). ZiFiT (Zinc Finger Targeter): an updated zinc finger engineering tool. Nucleic Acids Res. *38*, W462–W468.

Sanguinetti, M.C. (2010). HERG1 channelopathies. Pflugers Arch. *460*, 265–276.

Sanguinetti, M.C., and Jurkiewicz, N.K. (1990). Two components of cardiac delayed rectifier K+ current. Differential sensitivity to block by class III antiarrhythmic agents. J. Gen. Physiol. *96*, 195–215.

Sanguinetti, M.C., Jiang, C., Curran, M.E., and Keating, M.T. (1995). A mechanistic link between an inherited and an acquired cardiac arrhythmia: HERG encodes the IKr potassium channel. Cell *81*, 299–307.

Sarro, R., Kocher, A.A., Emera, D., Uebbing, S., Dutrow, E.V., Weatherbee, S.D., Nottoli, T., and Noonan, J.P. (2018). Disrupting the three-dimensional regulatory topology of the *Pitx1* locus results in overtly normal development. Development *145*, dev158550.

Scherrer-Crosbie, M., Ullrich, R., Bloch, K.D., Nakajima, H., Nasseri, B., Aretz, H.T., Lindsey, M.L., Vançon, A.C., Huang, P.L., Lee, R.T., et al. (2001). Endothelial nitric oxide synthase limits left ventricular remodeling after myocardial infarction in mice. Circulation *104*, 1286–1291.

Simonis, M., Klous, P., Homminga, I., Galjaard, R.J., Rijkers, E.J., Grosveld, F., Meijerink, J.P., and de Laat, W. (2009). High-resolution identification of balanced and complex chromosomal rearrangements by 4C technology. Nat. Methods *6*, 837–842.

Smemo, S., Campos, L.C., Moskowitz, I.P., Krieger, J.E., Pereira, A.C., and Nobrega, M.A. (2012). Regulatory variation in a TBX5 enhancer leads to isolated congenital heart disease. Hum. Mol. Genet. *21*, 3255–3263.

Stamatoyannopoulos, J.A., Snyder, M., Hardison, R., Ren, B., Gingeras, T., Gilbert, D.M., Groudine, M., Bender, M., Kaul, R., Canfield, T., et al.; Mouse ENCODE Consortium (2012). An encyclopedia of mouse DNA elements (Mouse ENCODE). Genome Biol. *13*, 418.

Teng, G.Q., Zhao, X., Lees-Miller, J.P., Quinn, F.R., Li, P., Rancourt, D.E., London, B., Cross, J.C., and Duff, H.J. (2008). Homozygous missense N629D hERG (KCNH2) potassium channel mutation causes developmental defects in the right ventricle and its outflow tract and embryonic lethality. Circ. Res. *103*, 1483–1491.

Trudeau, M.C., Warmke, J.W., Ganetzky, B., and Robertson, G.A. (1995). HERG, a human inward rectifier in the voltage-gated potassium channel family. Science *269*, 92–95.

van de Werken, H.J., Landan, G., Holwerda, S.J., Hoichman, M., Klous, P., Chachik, R., Splinter, E., Valdes-Quezada, C., Oz, Y., Bouwman, B.A., et al. (2012). Robust 4C-seq data analysis to screen for regulatory DNA interactions. Nat. Methods *9*, 969–972.

van den Boogaard, M., Smemo, S., Burnicka-Turek, O., Arnolds, D.E., van de Werken, H.J., Klous, P., McKean, D., Muehlschlegel, J.D., Moosmann, J., Toka, O., et al. (2014). A common genetic variant within SCN10A modulates cardiac SCN5A expression. J. Clin. Invest. *124*, 1844–1852.

van Duijvenboden, K., de Boer, B.A., Capon, N., Ruijter, J.M., and Christoffels, V.M. (2015). EMERGE: a flexible modelling framework to predict genomic regulatory elements from genomic signatures. Nucleic Acids Res. *44*, e42.

Xu, H., Guo, W., and Nerbonne, J.M. (1999). Four kinetically distinct depolarization-activated K+ currents in adult mouse ventricular myocytes. J. Gen. Physiol. *113*, 661–678.

Yue, F., Cheng, Y., Breschi, A., Vierstra, J., Wu, W., Ryba, T., Sandstrom, R., Ma, Z., Davis, C., Pope, B.D., et al.; Mouse ENCODE Consortium (2014). A comparative encyclopedia of DNA elements in the mouse genome. Nature *515*, 355–364.

STAR★METHODS

KEY RESOURCES TABLE

REAGENT or RESOURCE	SOURCE	IDENTIFIER
Chemicals, Peptides, and Recombinant Proteins		
DpnII	NEB	R0543M
Csp6I	ThermoFisher Scientific	ER0211
BsaI	NEB	R3535S
HindIII	NEB	R3104S
EcoRI	NEB	R3101L
T4 DNA Ligase	ThermoFisher Scientific	15224090
FBS	ThermoFisher Scientific	10270-106
Critical Commercial Assays		
TRIzol Reagent	Invitrogen	10296-010
Reliaprep RNA Tissue Miniprep System	Promega	Cat# Z6112
Superscript II system	ThermoFisher Scientific	Cat# 18064-071
Deposited Data		
Raw and analyzed data	This paper	GEO: GSE134725
Experimental Models: Cell Lines		
Mouse: HL-1	Claycomb et al., 1998	RRID:CVCL_0303
Human: HEK293T (female)	ATCC	Cat.#CRL-3216; RRID:CVCL_0063
Human: HepG2	ATCC	Cat.#HB-8065; RRID:CVCL_0027
Experimental Models: Organisms/Strains		
Mouse: FVB/NHanHsd	Envigo (Harlan)	N/A
Mouse: Kcnh2 CRE11$^{-/-}$	Amsterdam UMC, AMC	GM1619
Zebrafish: Strain, strain background (*D. rerio*), Tupfel long fin (TL)	ZIRC,Eugene or ZDB-GENO-990623–2	N/A
Oligonucleotides		
4C_Kcnh2_Prom_D-C_AdultHrt_Fw: AATGATACGGCGACCACCGAACACTCTTTCCCTACACGACGCTCTTCCGATCTGAGAGGTTTCTTCCTTTGGATC	Eurofins MWG Operon	N/A
4C_Kcnh2_Prom_D-C_AdultHrt_Rv: CAAGCAGAAGACGGCATACGAAAGCTCTCCTCAAGGCATTT	Eurofins MWG Operon	N/A
4C_Kcnh2_Prom_D-C_AdultLvr_Fw: AATGATACGGCGACCACCGAACACTCTTTCCCTACACGACGCTCTTCCGATCTCTGAGGTTTCTTCCTTTGGATC	Eurofins MWG Operon	N/A
4C_Kcnh2_Prom_D-C_AdultLvr_Rv: CAAGCAGAAGACGGCATACGAAAGCTCTCCTCAAGGCATTT	Eurofins MWG Operon	N/A
4C_Kcnh2_CRE11_D-C_AdultHrt_Fw: AATGATACGGCGACCACCGAACACTCTTTCCCTACACGACGCTCTTCCGATCTCTCTCTTCTAGCATGGCAGATC	Eurofins MWG Operon	N/A
4C_Kcnh2_CRE11_D-C_AdultHrt_Rv: CAAGCAGAAGACGGCATACGAGCTCCATGTGGGTAGGAATT	Eurofins MWG Operon	N/A
4C_Kcnh2_CRE11_D-C_AdultLvr_Fw: AATGATACGGCGACCACCGAACACTCTTTCCCTACACGACGCTCTTCCGATCTCTCTCTTCTAGCATGGCAGATC	Eurofins MWG Operon	N/A
4C_Kcnh2_CRE11_D-C_AdultLvr_Rv: CAAGCAGAAGACGGCATACGAGCTCCATGTGGGTAGGAATT	Eurofins MWG Operon	N/A
Primers for Kcnh2/CRE qPCR, TAD gene qPCR, ncRNA antisense oligonucleotides, and GapmeR and CRISPR sequences, are listed in Tables S2, S3, S4	N/A	N/A

(*Continued on next page*)

Continued

REAGENT or RESOURCE	SOURCE	IDENTIFIER
Recombinant DNA		
ZED vector	Bessa et al., 2009	N/A
pcDNA3.1(+) vector	Thermo Fisher Scientific	V79020
phRG-TK Renilla vector	Promega	Cat#E2231
pCS2FA-transposase	Kwan et al., 2007	N/A
Software and Algorithms		
LNA longRNA GapmeR design tool	Exiqon	N/A
ZiFit tool	Sander et al., 2010	N/A
Emerge	van Duijvenboden et al., 2015	https://www.medischebiologie.nl/files/
Occupeak	de Boer et al., 2014	https://www.medischebiologie.nl/files/
LinRegPCR	Ruijter et al., 2009	https://www.medischebiologie.nl/files/

LEAD CONTACT AND MATERIALS AVAILABILITY

Further information and requests for resources and reagents should be directed to and will be fulfilled by the Lead Contact, Vincent Christoffels (v.m.christoffels@amsterdamumc.nl).

EXPERIMENTAL MODEL AND SUBJECT DETAILS

Cell Lines and Culture Conditions

All cell lines were maintained in a 37°C incubator with 5% CO2. HL-1 (adult female atrial) cells were cultured in Claycomb medium supplemented with 10% chemically defined HL-1 FBS substitute (Lonza, 77227), 1% Glutamax (ThermoFisher Scientific, 35050-061) and 1% Pen/Strep (ThermoFisher Scientific, 15070-063). HEK293T (human, embryonic kidney, sex unknown) and HEPG2 (human, adolescent male liver epithelial) cells were cultured in DMEM (ThermoFisher Scientific, 31966-021) supplemented with 10% FBS (ThermoFisher Scientific, 10270-106) and 1% Pen/Strep (ThermoFisher Scientific, 15070-063).

Animals and *In Vivo* Procedures

Animals were maintained in accordance with the Guide for the Care and Use of Laboratory Animals published by the US National Institutes of Health (NIH Publication No. 85-23, revised 1996). All animal work was approved by the Animal Experimental Committee of the Academic Medical Center, Amsterdam, and carried out in compliance with the Dutch government guidelines. Fertilized FVB mouse oocytes were co-injected with Cas9 mRNA and sgRNA in a concentration of 25ng/μl Cas9 mRNA and 10ng/μl per sgRNA. Deletions were validated by PCR and Sanger sequencing. Founders were backcrossed with wild-type FVB mice to obtain stable lines. Downstream experiments were performed on F2 mice (both male and female), backcrossed twice with wild-type FVB mice. To obtain a murine RNA panel, total RNA was isolated from various tissues of wild-type adult mice (FVB/NHanHsd, Envigo (Harlan), both male and female), and RNA from embryonic tissues was isolated from CRE11$^{-/-}$ and wild-type littermate E17.5 fetuses (both male and female).

Study Approval

The investigation conforms to the Guide for the Care and Use of Laboratory Animals published by the US National Institutes of Health (NIH Publication No. 85-23, revised 1996). All animal work was approved by the Animal Experimental Committee of the Academic Medical Center, Amsterdam, and carried out in compliance with the Dutch government guidelines.

METHOD DETAILS

Identification of putative REs

Publicly available ChIP-seq datasets on cardiac transcription factors (TBX3, TBX5, TBX20, HEY2, MEF2, SRF), proteins associated with active regulatory elements (H3K4me1, H3K27ac, p300, DNaseI hypersensitivity marks (DHSs)(ENCODE Project Consortium, 2012; modENCODE Consortium et al., 2010; Stamatoyannopoulos et al., 2012), and active transcription (RNA polymerase 2, H3K4me3, H3K9ac, H3K36me3) were processed as described by the OccuPeak (de Boer et al., 2014) and EMERGE (van Duijvenboden et al., 2015) pipeline. In order to capture the maximum number of putative REs, we used a training dataset of validated heart and brain REs (true positive; TP) against random genomic DNA regions of 1 kbp (true negative, TN) to automatically assign weights to each dataset. After this, the datasets were merged and the RE predictions were exported to UCSC genome browser in a bedgraph

format. A detailed description of the EMERGE pipeline is available in the original publication (van Duijvenboden et al., 2015). 11 putative regions were selected to test for regulatory potential by luciferase assays and *in vivo* zebrafish assays as described below.

Cloning, Transfection and Luciferase assays

Reporter constructs were generated by ligating putative CREs (Table S1) to pGL2basic+minimal promoter (control reporter). HEK293T and were grown in 12-well plates in DMEM (ThermoFischer; 31966) supplemented with 10% FCS (GIBCOBRL) and 1% penicillin-streptomycin (ThermoFischer; 15070063). Transfection was performed polyethylenimine 25 kDa (PEI, Brunschwick) at a 1:3 ratio (DNA:PEI). HL-1 cells were grown in 12-well plates in Claycomb medium (Sigma-Aldrich; 51800C) supplemented with 1% FBS (GIBCOBRL), 1% Glutamax, 1% norepinephrine and 1% penicillin-streptomycin (ThermoFischer; 15070063). Transfection was performed using Lipofectamine 3000 (ThermoFischer; L3000015), according to manufacturer's protocol. Standard transfections used 1.4 μg of reporter (or control reporter) vector co-transfected with 3 ng phRG-TK Renilla vector (Promega) as normalization control. Transfections were carried out at least three times and measured in duplo. Luciferase measurements were performed using a Promega Turner Biosystems Modulus Multimode Reader luminometer. All data was statistically validated using an ANOVA two-way test.

In vivo zebrafish assay

All 11 CRE sequences were amplified by PhusionTAQ PCR (New England Biolabs, Ipswich, MA, USA) and cloned into the ZED vector (Bessa et al., 2009) by Gateway technology (Life Technologies BV, Bleiswijk, the Netherlands). The 11 ZED-CRE constructs were injected in WT zebrafish embryos at 1-cell stage at a final concentration of 15 ng/μl in presence of 25 ng/μl TOL2 transposase RNA. Embryos were kept at 28.5°C in E3 medium and scored for heart-specific RFP and subsequently heart-specific GFP fluorescence at 48 hpf on a Leica MZFLIII fluorescence stereomicroscope (Leica Microsystems GmbH, Wetzlar, Germany) set up with appropriate fluorescence filters. *In vivo* imaging of the embryos at 48 hpf was carried out on a Zeiss Axioskop 2 Mot plus fluorescence microscope (Carl Zeiss Micro Imaging GmbH, Jena, Germany) mounted with a Leica DFC490 CCD camera (Leica Microsystems) using appropriate fluorescence filters. Zebrafish hearts for each RE were scored for their expression of GFP, and percentages of GFP^+ hearts versus GFP^- hearts were calculated.

Preparation of 4C-template

4C templates were prepared as previously described (Simonis et al., 2009; van de Werken et al., 2012). In short, adult mouse hearts were isolated in ice cold PBS. Single cell suspensions were obtained by dissociation of tissue with IKA Ultra Turrax T5 FU, followed by dounce homogenization. Chromatin was cross-linked with 2% formaldehyde in PBS with 10% FCS for 10 min at room temperature, nuclei were isolated and cross-linked DNA was digested with a primary restriction enzyme recognizing a 4 bp restriction site (*DpnII*), followed by proximity ligation. Cross-links were removed and a secondary restriction enzyme digestion (*Csp6I*), followed again by proximity ligation. For all experiments, 200 ng of the resulting 4C template was used for the subsequent PCR reaction, of which 16 (total: 3.2 μg of 4C template) were pooled and purified for next-generation sequencing. The PCR products were purified using two columns per sample of the High Pure PCR Product Purification Kit (Roche cat. no. 11732676001). The kit separates the PCR products that are larger than 120 bp from the adaptor-containing primers (which are ~75 nucleotides (nt) and ~40 nt in size, respectively). Similar results were obtained with products from a single PCR reaction (200-ng template).

4C-seq primer design

PCR primers were designed based on the following criteria. The size of the viewpoint fragment was at least 500bp to allow efficient cross-linking to other DNA fragments. The fragment end (the region between the primary and secondary restriction enzyme) was more than 350 bp to allow efficient circularization during the second ligation step. Primers were designed to be maximally 20 nucleotides in length. The strategy therefore produces sequencing reads (36-mers in this study) composed of the 4C primer sequence (20 nucleotides, specific to a given viewpoint) followed by 16 nucleotides that identify a captured sequence. The reading primer always hybridizes to, and ends at, the 3′ side of the first restriction recognition site. This design ensures analysis of only primary ligation events and provides sufficient sequence information to unambiguously identify most captured sequences. The nonreading primers, with sizes of 18-20 nucleotides, were designed at a distance of $\leq$ 100 bp from the secondary restriction site. All primers had a GC-content between 35%–65% and an optimal basic temperature of 55°C, ranging from 45-65°C. Primers were checked against the mouse genome with MegaBLAST23 (settings -p 88.88 -W 12 -e 1 -F T), which requires primers on the reading side to be matched uniquely in the genome and primers on the nonreading side to have a maximum of three perfectly matching BLAST high-scoring segment pairs (HSP).

4C data analysis and statistics

4C templates were mixed and sequenced simultaneously in one Illumina HiSeq 2000 lane. The sequence tags generated by the procedure are prefixed by the 4C reading primer that includes the DpnII restriction site sequence (described in 4C primer design section). The 4C reading primer sequences are separated from multiplexed 4C-seq libraries and the suffixes are extracted for further processing. Mapping and filtering of the sequence reads was done as previously described (van de Werken et al., 2012). The algorithm constructs a background model for remote intra- and interchromosomal contacts to correct for systematic biases that

can occur during the 4C-seq experimental protocol. The algorithm is designed to use controls for sequencing errors and non-unique sequences while considering the high coverage (100x-100,000x) of fragment ends that are proximal to the viewpoint fragment. To normalize the interactions in close proximity to the viewpoint the algorithm was used to calculate the median of normalized coverage for running windows of size 4 kbp (depicted as black line) and sliding windows of 2-50 kbp of linearly increasing size (depicted as color-coded multiscale diagrams). All median values represent enrichment relative to the maximum attainable 4 kbp median value, whereas sliding windows represent enrichment relative to the maximum attainable 12 kbp median value. The 20th and 80th percentiles are also computed and depicted as the gray area around the 4 kbp running windows.

Quantitative expression analysis

To obtain a murine RNA panel, total RNA was isolated from various tissues of wild-type adult mice (FVB/NHanHsd, Envigo (Harlan)) using the TRIzol kit according to manufacturer's protocol (Invitrogen). Fetal atria, ventricles, brain, intestine, kidneys and livers of CRE11$^{-/-}$, and wild-type littermate E17.5 fetuses were isolated by microdissection, and total RNA was isolated using the Reliaprep RNA Tissue Miniprep System (Promega; Z6112). Subsequently, 1000ng total RNA was used for cDNA synthesis by reverse transcription using the Superscript II system (ThermoFisher Scientific; 18064-071). From the murine RNA panels, cDNA synthesis was performed using random hexamers. cDNA from fetal tissues was synthesized using oligo-dT oligonucleotides. Expression of genes and regulatory elements was assayed with quantitative real-time PCR using the Roche LightCycler 480 system. Primer sequences are listed in Table S2. Relative start concentration (N(0)) was calculated as previously described (Ruijter et al., 2009). Values were normalized to *Eef2* expression levels (Kouadjo et al., 2007)

Knockdown experiments using LNA^{TM} GapmeRs

LNA^{TM} GapmeRs against CRE11 transcript were designed by Exiqon using the LNA longRNA GapmeR design tool. Sequences are available in Table S3. HL-1 cells were cultured in 6-wells plates using Claycomb medium supplemented with 10% FCS (GIBCOBRL) and glutamine according to standard protocol. Upon transfection, HL-1 cells were maintained in antibiotics-free culture medium. GapmeRs were transfected using increasing concentrations of 1, 5, 25 and 50 μM. Four to 6 hours after transfection the culture medium was changed to culture medium with antibiotics. Cells were lysed 24 hours after transfection. RNA isolation and quantitative PCR were performed according to protocol described above. All experiments were performed in duplicate and repeated at least twice. To assess potential off-target effects, coding sequences of murine *Kcnh2a* and *Kcnh2b* were amplified from fetal heart-derived cDNA (described above). Primer sequences used for the amplification of cDNA are listed in Table S2. PCR products were cloned in between HindIII and EcoRI restriction sites of the pcDNA3.1(+) vector. Transfection of HEK293T cells with pcDNA-Kcnh2a and pcDNA-Kcnh2b expression vectors was performed as described above under **Cloning, Transfection and Luciferase assays**.

Generation of mutant mice

CRISPR target sites and oligonucleotides to generate single-guide RNAs (sgRNAs) flanking CRE11 were designed using the ZiFit tool (Sander et al., 2010). Target site and oligonucleotide sequences can be found in Table S4. sgRNA production was performed according to Cong et al. (Cong et al., 2013). CRISPR oligonucleotides were annealed for 5min at 95°C, and ligated in BsaI-digested pDR274 vector at room temperature for 2-3 hours using T4 DNA Ligase (Invitrogen). Ligation products were transformed on LB plates with Kanamycin. Colonies were checked by restriction analysis and sequencing for the uptake of the ligated product, and DNA from positive colonies was extracted by midiprep (Jetstar Kit; 200050). 3μg of the pDR274 expression vector was linearized with DraI for 4 hours at 37°C, and 3μg of the Cas9 expression vector was linearized with PmeI for 4 hours at 37°C. Linearized DNA was purified by phenol/chloroform extraction. sgRNA from DraI-digested sgRNA expression vector was transcribed using the MEGAshortscript T7 kit (Life Technologies; AM1354), and Cas9 mRNA from PmeI-digested Cas9 expression vector was transcribed using the mMessage mMachine T7 Ultra kit (Life Technologies; AM1345). sgRNA and Cas9 mRNA was purified using the MEGAclear kit (Life Technologies; AM1908). Fertilized FVB mouse oocytes were co-injected with Cas9 mRNA and sgRNA in a concentration of 25ng/μl Cas9 mRNA and 10ng/μl per sgRNA. Deletions were validated by PCR and Sanger sequencing. Founders were backcrossed with wild-type FVB mice to obtain stable lines. Downstream experiments were performed on F2 mice, backcrossed twice with wild-type FVB mice.

Chromosome Conformation Capture (3C)

3C was performed as described previously (Hagège et al.,2007) with minor modifications (Monroe et al., 2019). CRE11$^{+/+}$ and CRE11$^{-/-}$ hearts were isolated from adult mice and nuclei isolation and chromatin crosslinking was performed as described above (Preparation of 4C template). Crosslinked chromatin was digested with BglII (New England Biolabs; R0144S), yielding restriction fragments of > 1000bp and < 10.000bp. Digested chromatin was diluted and ligated overnight at 16°C with T4 DNA Ligase (Roche, #799009). DNA fragments were de-crosslinked overnight at 65°C, treated with Proteinase K and RNase A and purified by phenol/chloroform extraction and ethanol precipitation. Unidirectional qPCR primers targeting regions on the same strand were designed according to recommendations described previously (Naumova et al., 2012). Primer sites were designed ~80-150bp away from the restriction site to yield amplicons between 160 and 300bp in size. Primer sequences are listed in Table S5. Real-time quantitative PCR to quantify ligation frequencies was performed using SYBR Green (Roche; 4887352001) on a LightCycler 480 system. Ligation frequencies were normalized to a loading control (*Actb*; primer sequences in Table S2) and depicted as a ratio of ligation

frequencies of CRE11$^{-/-}$ over wild-type samples. Experiments were performed with 3 biological replicates per genotype and each measured in duplo.

QUANTIFICATION AND STATISTICAL ANALYSIS

Results are expressed as mean ± SEM. Details of the various statistical analyses can be found in the methods subsection of a specific experiment. In general, unless otherwise stated in the text or figure legend, significance refers to $p < 0.05$.

DATA AND CODE AVAILABILITY

The 4C-seq datasets generated during this study are available at GEO (https://www.ncbi.nlm.nih.gov/geo/) under accession number GEO: GSE134725.